

# Learning Diffusion Policies for Robotic Manipulation of Timber Joinery under Fabrication Uncertainty

Salma Mozaffari<sup>a, \*\*</sup>, Daniel Ruan<sup>a, \*\*</sup>, William van den Bogert<sup>b</sup>, Nima Fazeli<sup>b</sup>, Sigrid Adriaenssens<sup>a</sup>, Arash Adel<sup>a,\*</sup>

<sup>a</sup>*Princeton University, Princeton, NJ 08544, USA*

<sup>b</sup>*University of Michigan, Ann Arbor, MI 48109, USA*

## Abstract

Construction uncertainties such as fabrication inaccuracies and material imperfections pose a significant challenge to contact-rich robotic manipulation by hindering precise and robust assembly. In this paper, we explore the performance and robustness of diffusion policy learning as a promising solution for contact-sensitive robotic assembly at construction scale, using timber mortise and tenon joints as a case study. A two-phase study is conducted: first, to evaluate policy performance and applicability; second, to assess robustness in handling fabrication uncertainties simulated as randomized perturbations to the mortise position. The best-performing policy achieved a total average success rate of 75% with perturbations up to 10 mm, including 100% success in unperturbed cases. The results demonstrate the potential of sensory–motor diffusion policies to generalize to a wide range of complex, contact-rich assembly tasks across construction and manufacturing, advancing robotic construction under uncertainty and contributing to safer, more efficient building practices.

**Keywords:** Contact-rich manipulation, Robotic assembly, Fabrication uncertainty, Diffusion policy, Timber joinery, Robot learning, Construction robotics

## 1. Introduction

Construction plays a critical role in the global economy but continues to face long-standing challenges, including stagnant productivity growth, shortages of skilled labor, and persistent health and safety concerns [1, 2]. The industry often requires workers to perform repetitive and physically demanding tasks, such as lifting and positioning heavy components, which can contribute to chronic injuries and reduced long-term workforce capacity [3, 4]. Automation, and in particular robotic assembly, offers the potential to address these issues by enhancing precision, increasing efficiency, enabling mass customization, and reducing the physical burden on workers [5–7]. Recent advances in construction robotics have increasingly harnessed the precision and programmability of industrial robotic arms to execute complex and customized assemblies that would be difficult to achieve through manual methods [7, 8]. Despite these advancements, translating the capabilities of industrial robots from manufacturing to the uncertain and unstructured conditions of construction, characterized by fabrication inaccuracies,

material imperfections, as well as dynamic and evolving environments, remains a significant challenge, making it difficult to achieve the same levels of repeatability, quality, and precision that are standard in factory settings [1, 6, 9].

The momentum in construction robotics research is especially evident in recent work on robotic timber assembly [10–16], where many workflows rely on planar face-to-face or butt joints, whose geometric simplicity allows the use of pre-programmed trajectories for successful assembly. In contrast, the manipulation of traditional timber joinery such as mortise and tenon, lap, or scarf joints requires contact-sensitive insertion and interlocking, demanding high precision and control of contact forces [11, 17]. Similar to many contact-rich robotic manipulation tasks [18], the assembly of these joints can lead to misalignment and jamming if not coupled with real-time control for robust error recovery [19, 20]. As a result, these contact-sensitive tasks are often delegated to skilled human workers, who intervene to clamp, hammer, and adjust fits, compensating for fabrication inaccuracies and material imperfections [21]. While effective in the short term, such reliance on manual intervention can break the continuity of digital production workflows, introducing delays and reducing overall efficiency. Furthermore, it increases reliance on a shrinking pool of skilled labor and entails physically demanding, labor-intensive work that can contribute to worker fatigue and injury.

Timber joinery is a centuries-old construction technique of

\*Corresponding author.

\*\*Authors contributed equally to this work.

Email addresses: [salma.mozaffari@princeton.edu](mailto:salma.mozaffari@princeton.edu) (Salma Mozaffari), [daniel.ruan@princeton.edu](mailto:daniel.ruan@princeton.edu) (Daniel Ruan), [willvdb@umich.edu](mailto:willvdb@umich.edu) (William van den Bogert), [nfz@umich.edu](mailto:nfz@umich.edu) (Nima Fazeli), [sadriaen@princeton.edu](mailto:sadriaen@princeton.edu) (Sigrid Adriaenssens), [arash.adel@princeton.edu](mailto:arash.adel@princeton.edu) (Arash Adel)

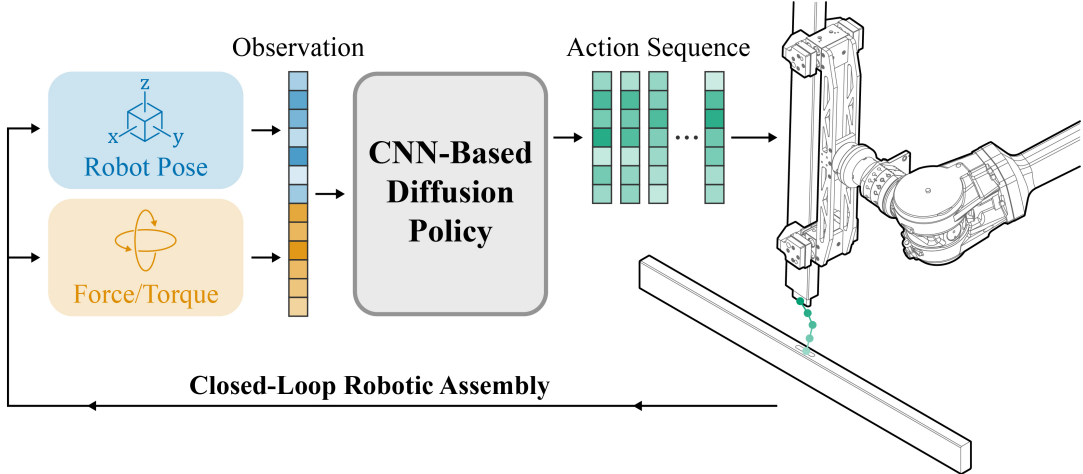


**Fig. 1.** Overview of our method. A CNN-based diffusion policy is trained conditional on end-effector pose and F/T data observations to predict sequences of robot actions.

geometrically interlocking timber components to create durable structural connections with minimal reliance on fasteners or adhesives [22]. These joints are valued for their enhanced structural performance, rotational stiffness, and resilience under seismic and fire conditions [23, 24]. While they offer significant structural advantages, their complex geometry and contact-rich assembly make them particularly sensitive to the uncertainties inherent to construction tasks, including fabrication inaccuracies from cut length and angle deviations and component shifting during picking, placing, and fastening, as well as material imperfections from dimensional variations and hygrothermal expansion [9]. Collectively, these factors further increase the complexity of automating the assembly of such joints in construction settings. Despite the significance of this challenge, automated assembly of traditional joinery remains nascent in robotic workflows within the Architecture, Engineering, and Construction (AEC) domain, particularly when accounting for fabrication and material uncertainty. Overcoming these limitations requires feedback-driven and closed-loop planning and control methods capable of adapting to unpredictable conditions inherent in construction workflows.

Learning-based methods have increasingly replaced traditional control-based methods for planning robot actions. Sensory–motor policy learning methods integrate sensor observations, planning, and control into a single end-to-end system, originally implemented using deep convolutional neural networks (CNNs) [25]. These methods enable the robot to learn how to act in response to what it senses without requiring separately engineered modules for perception, planning, state estimation, or low-level control. These learned control policies map raw observation inputs, such as force feedback and images captured from a camera, directly to motor commands or robot actions using various learning-based methods [26–29]. Among these methods, diffusion policy learning via behavior

cloning [30] has shown outstanding performance for various manipulation scenarios [31–34]. The key advantages of diffusion policies lie in their ability to learn multi-modal action distributions, capturing multiple plausible ways to perform a task, while maintaining training stability and predicting coherent sequences of future actions [30].

The research presented in this paper tackles the challenge of contact-rich robotic manipulation under construction uncertainties, where fabrication inaccuracies and material imperfections hinder precise and robust assembly. We address this by implementing diffusion policy learning, trained on robot pose and force/torque (F/T) data from teleoperated demonstrations, to plan and control the construction-scale assembly of mortise and tenon joints as a case study (Fig. 1).

### 1.1. Related work

In construction with discrete elements, such as brickwork and timber or steel framing, uncertainty remains a fundamental challenge to achieving precise and robust robotic assembly. In timber framing, which serves as the case study in this research, these uncertainties arise from material imperfections (e.g., dimensional deviations, deformation, shrinkage/expansion due to moisture) and fabrication inaccuracies (e.g., cut length and angle errors, pose deviations from calibration or handling). If unaccounted for, these variabilities accumulate during assembly, leading to misalignments, part collisions, and robot failures when trajectories are executed directly from as-planned digital models [9]. Prior research, in robotic timber assembly specifically, has explored various strategies to address these challenges, including the development of an external tracking system for end-effector pose correction in multi-robot assembly workflows [35], computational modeling of tolerance propagation [36], and adaptive, feedback-driven methods [9, 37–39]. The successful and precise execution of timber joints of

ten still depends on human intervention to correct deviations during nailing, gluing, and insertions [9, 10, 12, 13, 40]. The challenges of uncertainty become even more pronounced in contact-sensitive assembly tasks, such as those for traditional timber joinery, where success depends not only on geometric precision but also on the ability to control excessive force interactions imposed by friction and tight tolerances. In such scenarios, even minor deviations introduced during fabrication or caused by material imperfections can easily lead to misalignment, resulting in jamming, stick-slip behavior, and material damage [19].

Handling force interactions in contact-rich robotic manipulation is often addressed through model-based impedance or admittance control laws [41, 42], learning-based control policies [43, 44] or hybrid approaches combining both [32, 45]. In the context of assembly with timber joinery, a few studies have explored learning-based methods; Apolinarska et al. applied reinforcement learning for the motion control of an industrial robot to assemble single- and double-lap joints using robot pose and force/torque data from a wrist-mounted sensor [19]. For the single-lap tasks, they also investigated the policy robustness by introducing angular and linear offsets to the initial robot pose, grasping the top piece. Their results showed strong performance in zero-offset cases and revealed challenges of policy adaptation when angular and linear offsets, as well as angled or double insertions, were introduced. The findings underscored the importance of robust policy learning for handling geometric variations and positional deviations in contact-rich assembly tasks. Kramberger et al. also proposed a human–robot collaborative workflow using a learning-by-demonstration method that integrated a compliance controller into Cartesian-space dynamic movement primitives for perpendicular single-lap joint insertion; however, they relied on significantly loose tolerances [20].

Other studies have explored semi-structured or open-loop methods for timber joinery assembly; Robeller et al. introduced a custom end-effector that generated vibration combined with a manually applied pulse force using a mallet to facilitate the connection of timber panels using dovetail joints [46]. Leung et al. demonstrated the use of an industrial robot in combination with manually placed distributed robotic clamps to assemble tight-fitting half-lap joints, highlighting the potential for precise and repeatable assembly. During their experiments, they observed challenges such as misalignments and collisions—largely arising from fabrication inaccuracies and deviations between digital and as-built models—that are common in construction-scale robotic applications [17]. Rogeau employed visual feedback and fiducial markers for the assembly of wood panels with multiple mortise and tenon joints and reported successful full insertions in about 50% of their test cases across various joint configurations such as mortise tightness and tenon chamfer an-

gles [47].

Model-based control can be particularly difficult when handling complex contact dynamics, such as those found in multi-body and multi-surface interactions or in the manipulation of deformable objects. To overcome the challenges of model-based control, sensory–motor policy learning methods such as imitation learning, meta learning, self-supervised learning, and reinforcement learning are increasingly employed as effective alternatives [25–29]. These policies are trained to condition on sensor observations such as images and force feedback to produce robot actions. Among the learning methods mentioned, behavior cloning (a subcategory of imitation learning) is widely adopted, as it replaces task-specific robot programming with human demonstrations, typically collected through teleoperation [48–50]. Policy learning from human demonstrations can be perceived as a sequenced supervised learning problem that maps a history of observations to the sequence of actions (robot commands). With access to sufficient task demonstrations, behavior cloning has shown promise in tasks involving challenging conditions such as deformable objects and bimanual coordination [51, 52].

Diffusion policies [30, 52, 53] represent a recent class of behavior cloning methods built upon Denoising Diffusion Probabilistic Models (DDPMs) [54, 55] and Denoising Diffusion Implicit Models (DDIMs) [56]. DDPMs are generative models originally developed for high-quality image synthesis, transforming random noise into samples from a target distribution through an iterative denoising process. DDIMs extend this framework by formulating a non-Markovian reverse process, which allows the number of denoising steps used during inference to be reduced without changing the training procedure, thereby enabling significantly faster sampling. In the diffusion policy via robot action diffusion [30], the denoising process generates a sequence of robot trajectories at each inference step. The approach is known to naturally capture multimodal action distributions, meaning it can represent multiple distinct yet equally valid action sequences for completing a task, as often occurs in human demonstrations. The approach also maintains temporal coherence, meaning the policy predicts an entire sequence of future actions jointly rather than one step at a time. This joint prediction ensures that consecutive actions remain consistent (e.g., following one continuous path) rather than switching erratically between different predicted single actions, which can lead to unstable or jittery motion. Moreover, the method avoids the need for action discretization (breaking continuous movements into a fixed set of bins) or negative sampling (generating incorrect actions during training to guide learning) [30]. This removes common limitations of explicit behavior cloning methods [57, 58], which can make it difficult to achieve high-precision actions. Diffusion policies also offer improved training stability compared to implicit behavior

cloning methods [59, 60]. In addition, they have demonstrated robustness to perturbations, visual occlusions, and idle actions in some manipulation tasks [30].

Planning and control through contact remains a major challenge for both model- and learning-based approaches, due to the inherent complexity of contact dynamics [33]. While diffusion policies have achieved notable success in various dexterous manipulation tasks, their effectiveness in contact-rich scenarios is still under active investigation [32, 61, 62]. Additionally, despite significant progress in construction robotic research, the application of robot learning for planning and control, particularly for contact-sensitive tasks, remains underexplored. In this study, we evaluate the performance and robustness of diffusion policies through a case study on the assembly of timber mortise and tenon joints under fabrication uncertainty. The following section outlines the objectives, novelty, and contributions of this research.

### 1.2. Objectives and contributions

In the research presented in this paper, we develop a sensory-motor diffusion policy learning framework via behavior cloning for the contact-rich robotic manipulation at construction scale. The study pursues three primary objectives: (1) Demonstrate applicability and performance of diffusion policies through a case study on the robotic assembly of mortise and tenon timber joints; (2) Investigate policy robustness under construction-relevant uncertainties, simulated as randomized perturbations to the mortise position; and (3) Identify actionable guidelines for data collection strategies and policy parameter tuning that yield the most successful and robust performance, providing a practical reference for future research and deployment.

This paper presents one of the first systematic investigations in the AEC domain applying diffusion policy learning to robot planning and control. By enabling autonomous timber joinery assembly without reliance on hammering or human intervention, the proposed framework addresses physically demanding and craftsmanship-intensive tasks, offering a scalable learning framework for contact-sensitive manipulation tasks. The approach demonstrates potential for generalizing a wide spectrum of contact-rich assembly challenges, including complex timber joints, pipe fitting, and light metal framing. Ultimately, this work contributes to advancing robotic construction under uncertainty, bridging state-of-the-art generative policy learning with real-world AEC workflows, and provides both theoretical and practical advances that can accelerate adoption across the field.

## 2. Methods

This section outlines the experimental setup, data collection process, policy learning approach, and evaluation procedure used in our robotic manipulation system for timber joinery. We

implement diffusion policy learning via behavioral cloning using robot pose and F/T data collected from teleoperated demonstrations.

### 2.1. Experimental setup

Our experimental setup consists of two primary systems for conducting this research. The first is a multi-robot setup equipped with customized end effectors for executing the timber assembly task. The second is a teleoperation system for manually operating the robotic setup and collecting data for demonstrations. This subsection details the specific hardware used for our experiments and their software interfaces.

The multi-robot setup consists of two 6-axis industrial robotic arms<sup>1</sup>, each with a 40 kg payload and a 2.55 m reach mounted on linear tracks (Fig. 2). Both robotic arms utilize custom pneumatically-driven end effectors designed for gripping long timber elements with varying cross-sectional profiles, as typically encountered in timber frame construction. One arm grasps the timber mortise in place and can systematically simulate construction deviations by adding positional offsets. The other arm grasps the timber tenon and is the primary agent for manipulation and completing the assembly task.

Because the industrial robotic arms do not provide native access to joint torque values, we developed the end effector on the tenon-grasping arm to include a 6-axis F/T sensor<sup>2</sup> to enable F/T data collection (Fig. 3). For safety, the end effector is also equipped with a pneumatic anti-collision sensor<sup>3</sup>, which both provides passive mechanical compliance and triggers a protective stop on the robotic arm under excessive force, safeguarding the robotic setup and F/T sensor. Motion control and pose feedback for the robotic arms utilize ABB’s Externally Guided Motion (EGM) feature [66], a UDP-based real-time control interface. F/T data is transferred over EtherCAT to a central Programmable Logic Controller (PLC)<sup>4</sup>. All data communications are centralized on a desktop computer employing ROS<sup>5</sup> interfaces and Python wrappers.

The teleoperation system (Fig. 4) consists of a virtual reality (VR) system<sup>6</sup>, and we developed a unilateral pose-to-pose transformation from the VR controller to the robotic arm’s end effector. This transformation is essential for aligning the coordinate frames of the VR system and the robotic setup, and for compensating for the human demonstrator’s orientation relative to the robot. For instance, when the demonstrator is facing the robotic arm, pushing the controller forward should consistently move the end effector away from the demonstrator, re-

<sup>1</sup>ABB IRB 4600 [63]

<sup>2</sup>ATI Delta IP60, with SI-330-30 calibration [64]

<sup>3</sup>Schunk OPR 081-P00 [65]

<sup>4</sup>Beckhoff CX2062 [67]

<sup>5</sup>ROS 2 Jazzy Jalisco [68]

<sup>6</sup>HTC VIVE Pro 2 [69]

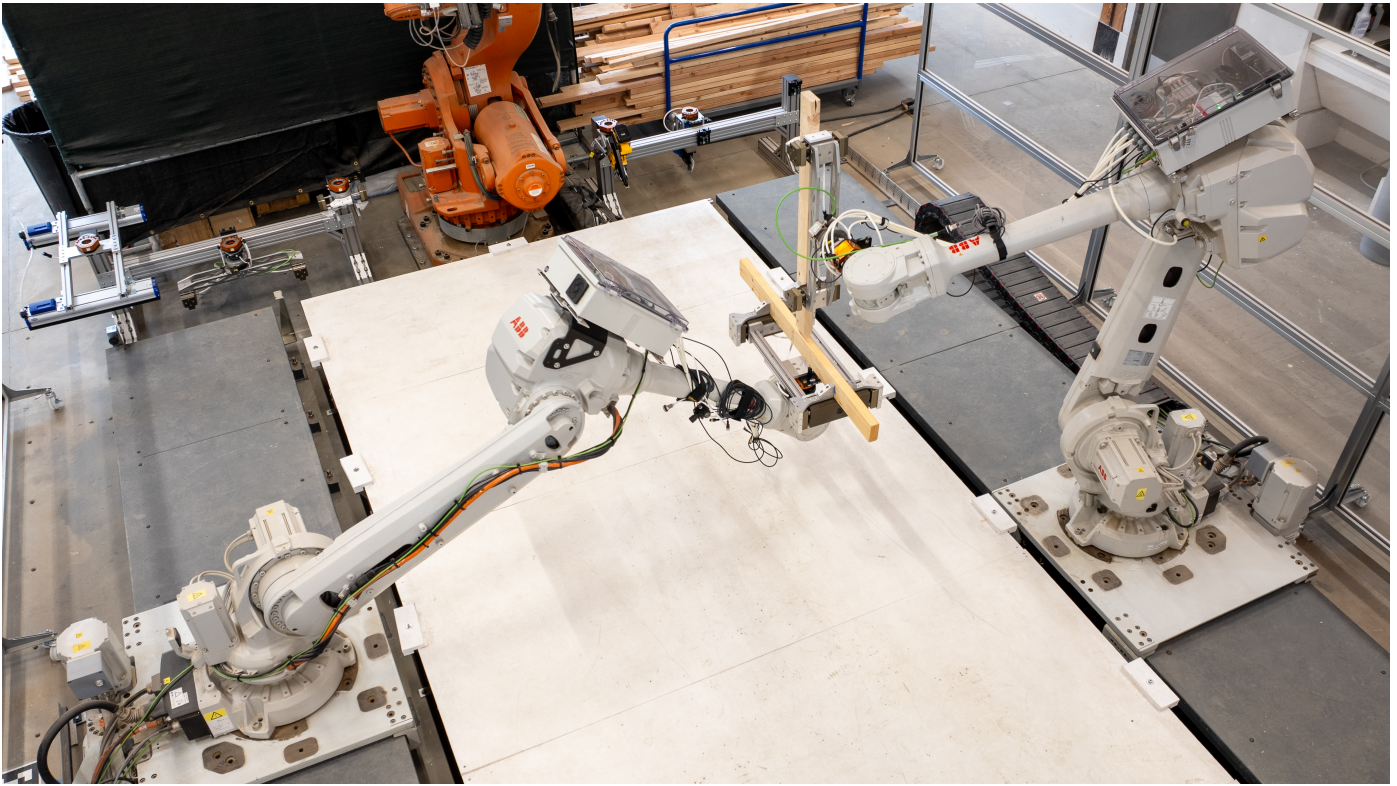


**Fig. 2.** Multi-robot setup consisting of two 6-axis industrial robotic arms.

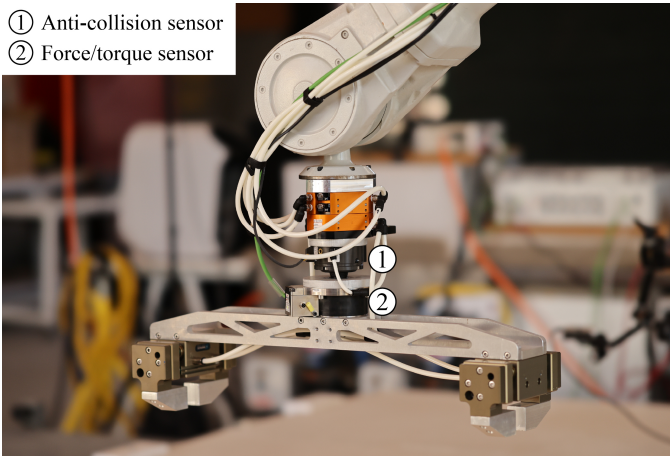


**Fig. 3.** Gripper for holding the tenon piece equipped with anti-collision and F/T sensors.

gardless of their position. In addition, this transformation includes an adjustable scaling parameter that maps the demonstrator's control motions to proportionally smaller movements on the robot, enhancing the demonstrator's fine motor control capabilities during high-precision tasks such as timber joint assembly. During teleoperation, robot motion and data collection (see Section 2.2) are enabled by the hand controller's trigger. Similar to clicking and dragging a mouse, holding the trigger moves the robot in the desired direction, and releasing it allows the controller to be repositioned without affecting the robot or

recording idle data. This allows for long motions to be performed in smaller, controlled segments. The VR controller interface utilizes OpenVR [70] in Python and ROS, integrating directly with the multi-robot setup by streaming mapped poses to EGM for fluid, real-time teleoperation.

## 2.2. Data collection

To train our diffusion policies, we created datasets consisting of expert demonstrations. An overview of the data collection workflow is illustrated in Fig. 5. During data collection, a human demonstrator utilized the teleoperation system to manipulate a vertical tenon into the mortise. The demonstrator initiates the task by simultaneously straightening the tenon and executing a downward motion to guide it into the mortise. To improve the robustness of the learned policy under fabrication uncertainties, we dedicated approximately 25% of the demonstrations to error recovery scenarios. In these cases, the demonstrator intentionally initiates contact with the edges of the mortise and performs a sliding maneuver along the surface to realign and insert the tenon, mimicking realistic recovery behaviors in the presence of misalignment. Each collected demonstration consists of timestamped robot poses and F/T data during motion (while the VR controller's trigger is held).

The raw data for each demonstration is recorded in real-time for each sensor interface: pose data is collected from EGM as a seven-dimensional (7D) vector (3D position in millimeters +



**Fig. 4.** VR-based teleoperation system for collecting human expert demonstrations.

4D quaternion rotation of the tenon gripper end effector) every 12 ms (approximately 83 Hz), while F/T data is collected as a 6D vector (3D force in newtons + 3D torque in newton-meters) at 64 Hz after passing through an infinite impulse response (IIR) low-pass filter to attenuate frequency components above 64 Hz. This filtering step mitigates aliasing and improves signal quality by removing sensor noise and dynamic vibrations introduced by high-speed motion or structural resonances. To temporally align the different sample rates to a common time base, the pose and F/T data are interpolated to 60 Hz; position and F/T data are linearly interpolated, while rotation data uses spherical linear interpolation to preserve smooth interpolation.

Finally, each episode is post-processed to reduce unwanted noise in the demonstrations and remove periods of inactivity or unintentional stillness. Removing idle or near-idle periods is critical as it helps the policy training to focus on active, meaningful interactions rather than noise or moments where no significant movement occurs. We filter the pose and F/T data using a low-pass Butterworth filter [71], with filter parameters selected to reduce unwanted high-frequency noise while preserving the underlying movement patterns (Fig. 6). For the pose data, we used a 4th-order low-pass Butterworth filter with a 1 Hz cutoff, which provides a steeper roll-off and ensures that only low-frequency components characteristic of slower, continuous motion trajectories remain. In contrast, we used a 1st-order low-pass Butterworth filter with a higher 10 Hz cutoff to preserve sharper transitions (e.g., at the moment of contact)

while effectively removing high-frequency noise that may come from mechanical oscillations or sensor inaccuracies. Actions are then derived from finite differences between successive pose data points, and any resulting vectors with magnitudes below a set threshold are removed to discard idle or near-idle actions.

### 2.3. Policy learning

Our research employs CNN-based diffusion policy learning via behavioral cloning [30]. The method is based on DDPMs [54, 55] and DDIMs [56], using DDPM for the forward noising process during training and DDIM for the reverse denoising process and faster inference during rollouts. Our diffusion policies predict a sequence of robot actions (i.e., the robot pose) conditional on the observation horizon of robot pose and F/T data. The foundation for our diffusion models is built upon the work of Bogert et al. [72].

When loading the dataset for training our diffusion policies, trajectories of 64 points are subsampled from each demonstration. This subsampling normalizes the trajectory length for each demonstration, as well as enables faster training iterations. Next, we converted pose quaternions to a continuous 6D rotation representation (by first converting to rotation matrices then concatenating the first two columns) to improve training stability [30, 73], resulting in 9D pose vectors. We then applied min-max normalization to scale all features to the range [-1, 1]. Given a pose observation horizon  $T_o^p$ , F/T observation horizon  $T_o^f$ , and action prediction horizon  $T_p$ , each training sample at timestep  $t$  consists of an observation feature  $\mathbf{O}_t$  concatenating the last  $T_o^p$  and  $T_o^f$  and a corresponding action sequence  $\mathbf{A}_t$  consisting of the next  $T_p$  absolute poses.

During the rollouts,  $\mathbf{A}_t$  is predicted conditioned on  $\mathbf{O}_t$ . The reverse denoising process for action prediction starts from  $\mathbf{A}^K$  sampled from Gaussian noise. After iterating  $K$  denoising steps, we output a desired noise-free action  $\mathbf{A}^0$  at step 0. The action at each reverse step  $k - 1$  is calculated as [30]:

$$\mathbf{A}_t^{k-1} = \alpha \left[ \mathbf{A}_t^k - \gamma \epsilon_\theta + \mathcal{N}(0, \sigma^2 I) \right] \quad (1)$$

where  $\epsilon_\theta$  is the learned predicted noise and  $\mathcal{N}(0, \sigma^2 I)$  is Gaussian noise. The  $\alpha$ ,  $\gamma$ ,  $\sigma$  are functions of the iteration step  $k$  and are defined through a selected noise schedule. In our case, a squared cosine noise schedule [74] is used. The noise prediction network  $\epsilon_\theta$  is learned using a 1D CNN U-Net architecture by minimizing the following mean squared error (MSE) loss [30]:

$$\mathcal{L} = \sum \left\| \epsilon^k - \epsilon_\theta(\mathbf{O}_t, \mathbf{A}_t^k, k) \right\| \quad (2)$$

where  $\epsilon^k$  is the sampled random noise with known variance at iteration  $k$ . The predicted noise  $\epsilon_\theta(\mathbf{O}_t, \mathbf{A}_t^k, k)$  is a function of  $\mathbf{O}_t$ , the pose and F/T observation feedback preceding time  $t$ ,  $\mathbf{A}_t^k = \mathbf{A}^0 + \epsilon^k$  with  $\mathbf{A}^0$  sampled from starting noise-free actions, and

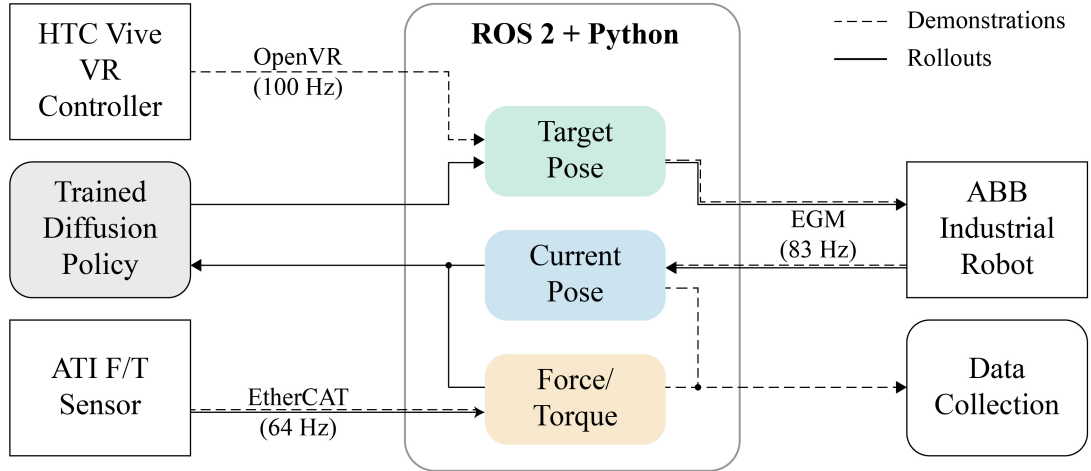


**Fig. 5.** Data collection and policy rollout workflow.

iteration step  $k$ . As implemented in [30], we add the sampled random noise  $\epsilon^k$  to the noise-free actions  $\mathbf{A}_0$  in  $K$  forward steps (original DDPM method).

Policy training was conducted on high-performance computing (HPC) clusters<sup>7</sup>, which provide powerful computational resources for efficiently processing large datasets and enabling faster, scalable learning by leveraging parallel computing capabilities. Each policy was trained for a fixed amount of time (1 hour), with each training lasting at least 1,000 epochs. Only the model weights corresponding to the epoch with the lowest validation loss were used to evaluate performance during rollouts. To account for training variance, we trained 4 models for each set of parameters and averaged their success rates when computing their performance (see Section 2.4).

#### 2.4. Evaluation

To evaluate the performance of our trained policies, we perform rollouts on the experimental setup (Section 2.1). The starting position for the tenon piece during all rollouts is fixed and identical to the demonstrations. During policy rollouts, we specify additional parameters for the number of inference steps  $K_{\text{inf}}$ , DDIM/DDPM interpolation  $\eta$  [56], and action execution steps  $T_a$ . The number of inference steps ( $K_{\text{inf}} \leq K$ ) controls the number of steps in the reverse denoising process during policy inference. Decreasing  $K_{\text{inf}}$  reduces computation and increases rollout speed, which is important for real-time policy execution. However, smaller  $K_{\text{inf}}$  may also reduce the quality of noise sampling or action precision.

The amount of stochasticity during the reverse denoising process is controlled by the interpolation parameter  $\eta \in [0, 1]$ , where  $\eta = 0$  is the DDIM process and  $\eta = 1$  is the original

DDPM process. This means that when  $\eta = 0$ , the standard deviation of the noise added during sampling is 0, meaning that the reverse process is fully deterministic, producing high-fidelity imitations of demonstrations, and when  $\eta = 1$ , the reverse process is fully stochastic, introducing broader behavioral coverage with exploration and variability.

The number of action execution steps  $T_a \leq T_p$  denotes that of the  $T_p$  predicted actions at each time step; we execute the first  $T_a$  actions. Decreasing the value of  $T_a$  increases the frequency of replanning over a receding horizon, increasing the responsiveness of the system; however, it can also potentially decrease the speed of rollouts by spending more time on inference. For values of  $T_a > 2$ , we apply an average pooling with a kernel size of  $T_a - 1$  across each dimension of the actions, smoothing the action sequence.

In contrast to data collection during demonstrations, observations during rollouts are not temporally aligned and instead utilize the latest available pose and F/T data when the observation is retrieved. These observations are normalized using the same normalization parameters as the dataset before being passed to the policy for inference. The output action sequence is similarly denormalized back into the original scale using the same action normalization parameters during training. These predicted actions are then sent through EGM to the robot controller, and we use a similar communication protocol to the data collection to receive pose and F/T feedback (see Fig. 5).

The policy performance is determined by rolling out 5 times for each of the 4 trained models with fixed parameters, to account for stochasticity during test time, resulting in an average success rate (Avg. SR) across 20 combined rollouts. A rollout is recorded as a success if the tenon element fully inserts into the mortise hole without triggering any collision errors (i.e., excessive force at either the collision sensor or the robot joints).

<sup>7</sup>Princeton Research Computing’s Della cluster

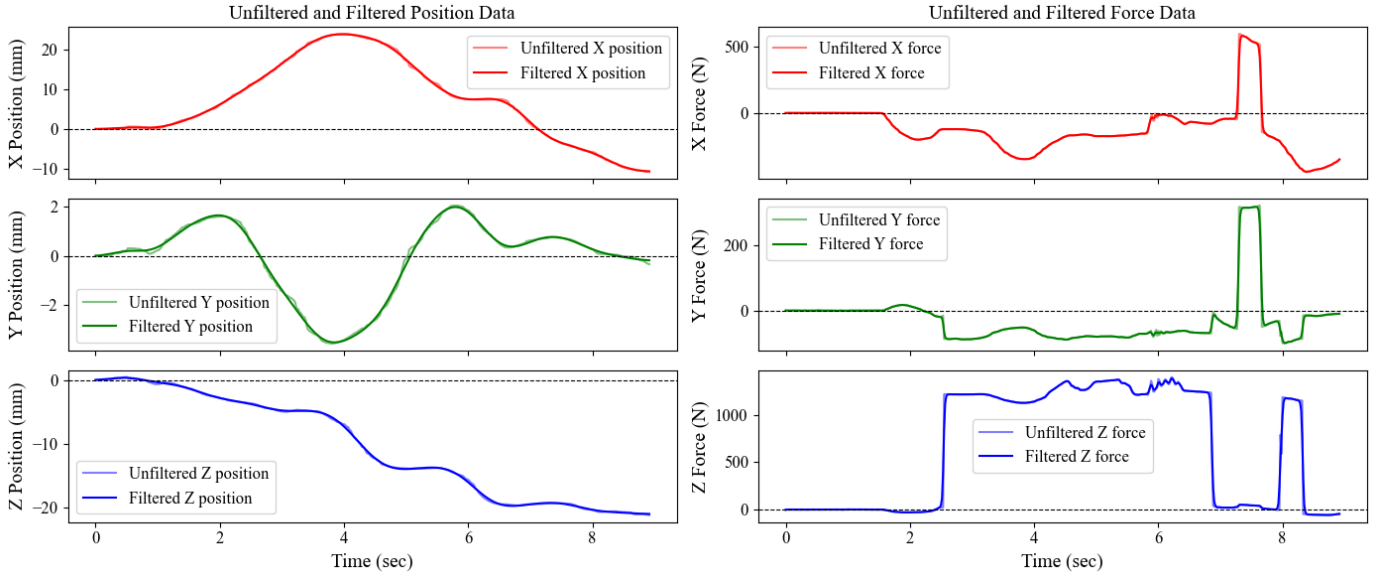


**Fig. 6.** Data filtering using a low-pass Butterworth filter. The visualized trajectory is for an error recovery scenario, demonstrating insertion after a collision with the mortise surface. Only the first 3 dimensions for each pose and F/T data are shown.

A rollout is recorded as a failure if any collision errors are triggered by the industrial robot controller or if the policy does not appear to be making any meaningful progress towards task completion, as determined by the operator.

### 3. Experiments

We conducted a two-phase study: in Phase 1 we performed static experiments with a fixed mortise location to establish a general performance evaluation for the diffusion policy in our industrial setup; in Phase 2 we performed uncertainty experiments with randomized hole offsets to evaluate the robustness of the diffusion policies.

The dimensions of the mortise and tenon we used for the experiments are illustrated in Fig. 7. The tolerance between the tenon cheeks and the mortise walls was 0.1 mm, and the tolerance between the tenon edges and the mortise walls was about 2 mm. The tight tolerance of the tenon cheeks is what ensures a structural fit for a mortise and tenon joint. This figure also visualizes the boundary of the 5 mm and 10 mm offsets used in the uncertainty experiments (see Section 3.2). The tenon is aligned along the world's z-axis, while the mortise piece lies horizontally along the x-axis. Each demonstration and rollout begins with the tenon element grasped at a fixed starting pose, positioned approximately 15 mm vertically above the mortise hole with an approximately 6° angular deviation about the y-axis.

#### 3.1. Phase 1: Static experiments

The objective of the Phase 1 experiments is to show the application and performance of diffusion policies in a building-scale robotic assembly setting. For this experiment, we cre-

ated a dataset of 100 demonstrations following the data collection method described in Section 2.2, with the exception that no demonstrations included error recovery cases and demonstrations were not post-processed. To simplify the assembly task, the mortise position was held fixed across all demonstrations and during rollouts. Through repeated experimentation, we identified the best-performing set of parameters (reported in Section 4.1), which were then used to initialize parameter tuning in the Phase 2 experiments described in the following subsection.

#### 3.2. Phase 2: Uncertainty experiments

The objective of the Phase 2 experiments is to demonstrate the robustness of diffusion policies in handling fabrication uncertainties for contact-rich timber joinery. More specifically, we evaluate how the policies perform when the mortise is subjected to random position offsets simulating fabrication tolerances.

We created a dataset of 400 demonstrations following the data collection method outlined in Section 2.2. To simulate fabrication tolerances, the position of the mortise in these demonstrations was perturbed by a displacement vector sampled in polar coordinates. The angular component was drawn uniformly from  $[0, 2\pi]$  radians, and the radial component was drawn uniformly from  $[0, 10]$  mm. Unlike uniform sampling over the area of a disk, this approach yields a higher density of samples near the origin, biasing the distribution toward smaller offsets while still allowing for the possibility of larger deviations.

During rollouts, we evaluated each policy at three goal offset distances: 0 mm (no offset), 5 mm, and 10 mm. These values were selected to evaluate the policies under no uncertainty (0 mm), uncertainty within the demonstration distribu-

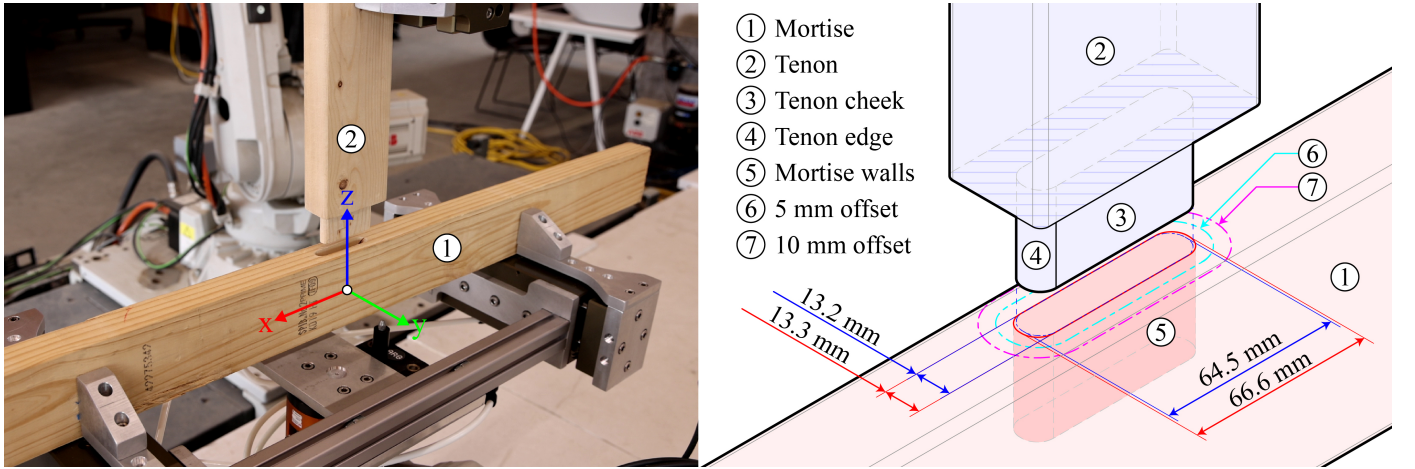


Fig. 7. Mortise and tenon terminology, dimensions, and reference frame.

tion (5 mm), and uncertainty at the edge of the demonstration distribution (10 mm). For each offset condition, the goal position was randomized uniformly along the circumference of a circle with a radius of the specified distance. The success rate of a policy was computed separately for each offset distance, and its overall performance was reported as the average success rate across all three conditions.

In the first part of the Phase 2 experiments, we systematically tuned the parameters of the diffusion policy to maximize the success rate. Starting from a candidate configuration derived from the Phase 1 experiments (Section 3.1), we performed sequential, greedy parameter tuning, optimizing one parameter at a time while holding others fixed. The resulting best-performing policy is referred to as the full model. The impact of individual parameters on policy performance is reported in Section 4.2.1.

In the second part of the Phase 2 experiments, we conducted two ablation studies to assess the impact of F/T observations and demonstration count on policy performance. In the F/T ablation study, we evaluated the performance of the full model with F/T inputs masked (i.e., input F/T values are set to 0), as well as a variant trained using only pose observations. For the demonstration ablation, we trained policies using 25, 50, 100, and 200 demonstrations, while keeping all other parameters identical to the full model. The results of these studies are presented in Sections 4.2.2 and 4.2.3.

## 4. Results and discussion

Across all experiments, policy training exhibited consistent and stable convergence. Training and validation MSE losses remained closely aligned throughout policy training, suggesting minimal overfitting. Both losses decreased steadily over the first 300 epochs, followed by a gradual plateau beginning at approximately 600 epochs. An example of the MSE loss curves

is illustrated in Fig. 8 for the full model (see Section 4.2.1). The loss curves were first averaged across all 4 training iterations, then smoothed using a Gaussian filter with a standard deviation  $\sigma = 10$  for visualization.

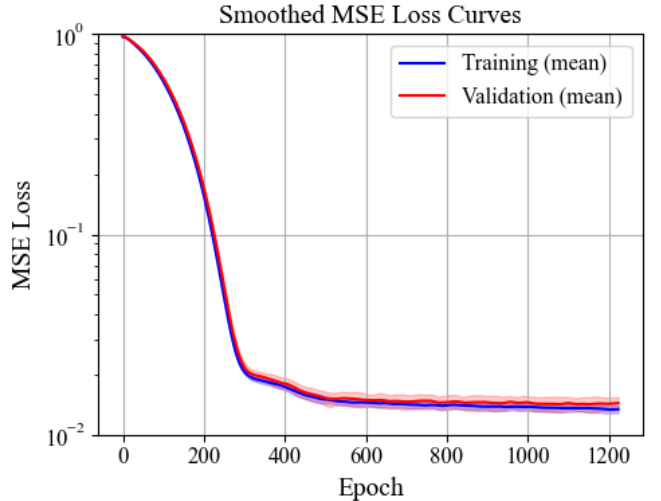
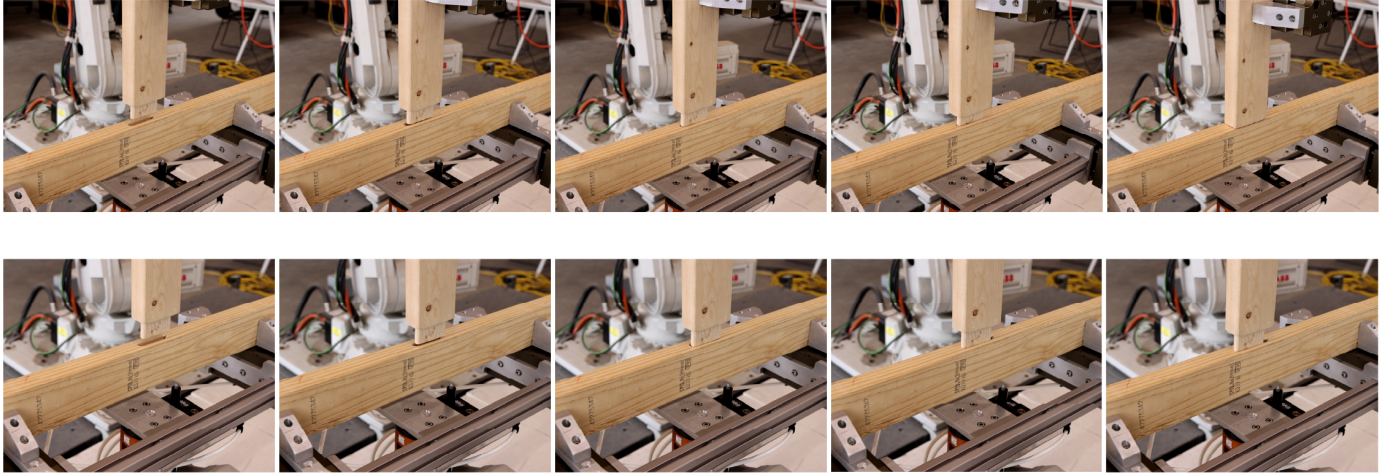


Fig. 8. Smoothed mean squared error (MSE) training and validation loss curves for Policy 4, averaged then smoothed across all training iterations. The shaded area represents  $\pm 1$  standard deviation.

Fig. 9 illustrates two example rollout trajectories: the top sequence shows a successful rollout where the tenon was first re-oriented and then smoothly inserted into the mortise; the bottom sequence shows an unsuccessful rollout where the tenon did not finish reorienting before hitting the edge of the mortise and was unable to recover correctly.

### 4.1. Phase 1: Static experiments

After repeated testing and parameter tuning, the policy achieved a 100% average success rate over 20 rollouts using the parameter values listed in Table 1. This performance demonstrates the capability of diffusion policies to reliably assemble



**Fig. 9.** Example of an insertion sequence for a successful rollout (top row) and an unsuccessful rollout (bottom row).

a timber mortise and tenon joint under no uncertainty. These parameter values were subsequently used as the initialization point for parameter tuning in the Phase 2 experiments.

**Table 1.** Parameters for the Phase 1 experiments.

Symbol	Description	Value
$L_r$	Learning rate	1e-5
$W_d$	Weight decay rate	1e-6
$T_o^p$	Pose observation horizon	1
$T_o^f$	Force observation horizon	1
$T_p$	Action prediction horizon	8
$T_a$	Action execution steps	4
$K$	Forward noising steps	128
$K_{\text{inf}}$	Inference/denoising steps	32
$\eta$	DDIM/DDPM interpolation	0.5

During the first phase of the experiments, we also evaluated encoder networks for pose and F/T inputs to the diffusion policy. Each encoder consisted of a single fully connected layer that projected the raw input vector to a latent representation of fixed length (e.g., 64 or 128 units). The aim was to learn a compact feature embedding prior to policy integration. However, policies incorporating these encoders underperformed relative to those that directly concatenated the unprocessed pose and F/T observations. Future research may explore the impact of more sophisticated encoders, such as multi-layer, frequency-based, or attention-based architectures, on policy performance [32, 75].

The Phase 1 experiments also revealed several practical challenges that we addressed during the Phase 2 experiments. First, as the human demonstrator became increasingly familiar with the setup, the demonstrations tended to become faster and more fluid over time. Although random sampling during dataset construction mitigated this effect, the demonstrations lacked examples of mistakes and error recovery for the policy to learn from.

This limitation was later addressed in our revised data collection procedure (Section 2.2), in which a specified percentage of demonstrations was deliberately dedicated to error recovery scenarios.

A second challenge arose from the gradual physical degradation of the experimental setup as a consequence of the large construction-scale forces repeatedly exerted on the timber mortise and tenon. This degradation manifested in several ways: wear on contact surfaces (increasing tolerance and making insertion easier), small chips breaking off the tenon edge (slightly decreasing tolerance due to glue reattachment), and minor shifts of the mortise and tenon within the gripper grasp. Such occurrences are expected in real-world construction environments, but they also introduce additional sources of uncertainty. Future research should explicitly account for these fabrication-induced variations when developing and evaluating assembly policies.

## 4.2. Phase 2: Uncertainty experiments

### 4.2.1. Full model parameter tuning

The sequential parameter tuning in Phase 2 was limited to three stages: (1) pose and F/T observation horizons; (2) action prediction horizon; (3) number of inference steps and DDIM/DDPM interpolation. The learning rate, weight decay, and forward noising steps were fixed at the values determined in Phase 1.

Table 2 summarizes the results from the first two stages. The highest average total success rate of 75%, computed over the three mortise offset conditions, was achieved using an observation horizon of 1 for both pose and F/T modalities combined with a longer action prediction horizon of 16. This configuration suggests that, for the uncertainty conditions tested, the policy benefited from focusing on the most recent state information while planning actions further into the future, potentially allowing it to better anticipate and correct for deviations introduced by positional offsets.

**Table 2.** Success rates for training parameter tuning.

Policy	# Demos	$T_p$	$T_o^p$	$T_o^f$	$K_{\text{inf}}$	$\eta$	$T_a$	D (mm)	Avg. SR (%)	Avg. total SR (%)
1	400	8	1	1	32	0.5	4	0	90	70
								5	55	
								10	65	
2	400	8	2	1	32	0.5	4	0	85	63
								5	65	
								10	40	
3	400	8	2	2	32	0.5	4	0	80	60
								5	60	
								10	40	
4	400	16	1	1	32	0.5	8	0	100	75
								5	65	
								10	60	

D = randomized hole offset.

Table 3 summarizes the final stage of rollout parameter tuning, evaluating different combinations of inference steps and DDIM/DDPM interpolation values. These tests were conducted only for mortise offsets of 5 mm. The initial parameter values selected from the Phase 1 experiments achieved the highest performance, with a 65% average success rate, substantially outperforming other tested configurations.

#### 4.2.2. Force/torque ablation study

Table 4 summarizes the results of the F/T ablation study, and Fig. 10 illustrates the contribution of F/T feedback to task performance. As expected, both ablated policies underperformed relative to the full model. However, a notable pattern emerged when comparing the pose-only policy to the masked full model. When F/T inputs were masked in the full model, the tenon consistently collided with the mortise, reflecting the model’s inability to detect contact without force feedback. Surprisingly, the pose-only policy occasionally succeeded under the 10 mm mortise offset condition, despite lacking force information. The large standard error in model variance (Fig. 10) for this condition suggests that these successes were likely the result of random factors rather than reliable inference. This highlights the critical role of force feedback in consistent policy performance, particularly under larger fabrication uncertainties.

#### 4.2.3. Demonstration quantity ablation study

Table 5 summarizes the results of the demonstration quantity ablation study. Policies trained on only 25 demonstrations failed to fully converge and achieved no success during rollouts, and were therefore excluded from the reported results. Fig. 11 shows a pronounced drop in success rate at the 10 mm mortise offset when the number of demonstrations was reduced, likely due to insufficient coverage of the state-action space in

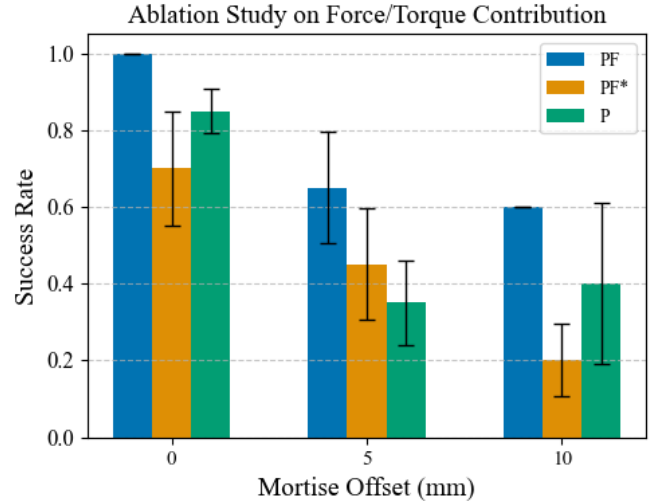


**Fig. 10.** Success rates of diffusion policies with force masked (PF\*) and trained only on pose data (P) compared to the full model (PF), evaluated at three mortise offsets (0, 5, and 10 mm). Error bars indicate the standard error of the mean (SEM) computed across the 4 independently trained models for each set of parameters.

the demonstration data. The results suggest a performance inflection point between 200 and 400 demonstrations, beyond which the policy gains a substantial improvement in its ability to handle positional uncertainty. This trend indicates that under higher uncertainty, diffusion policies may require a critical mass of demonstrations to adequately represent recovery behaviors.

Notably, the total number of demonstrations required to achieve robust performance was much higher than anticipated. This is likely attributable to the trajectory subsampling strategy used during policy learning (Section 2.3), which significantly reduced the total number of training samples available to the

**Table 3.** Success rates for rollout parameter tuning.

Policy	# Demos	$T_p$	$T_o^p$	$T_o^f$	$T_a$	D (mm)	$K_{\text{inf}}$	$\eta$	Avg. SR (%)
4	400	16	1	1	8	5	32	0.5	65
							16	0.5	35
							64	0.5	40
							32	1	35
							32	0.25	50

D = randomized hole offset.

**Table 4.** Success rates for the F/T ablation study.

Policy	Modality	# Demos	$T_p$	$T_o^p$	$T_o^f$	$K_{\text{inf}}$	$\eta$	$T_a$	D (mm)	Avg. SR (%)	Avg. total SR (%)
4	PF	400	16	1	1	32	0.5	8	0	100	75
									5	65	
									10	60	
4	PF*	400	16	1	1	32	0.5	8	0	70	45
									5	45	
									10	20	
9	P	400	16	1	1	32	0.5	8	0	85	53
									5	35	
									10	40	

D = randomized hole offset; PF = models trained with pose and force data; P = models trained with pose-only data.

\*The forces were masked during rollouts.

policy. Future research should utilize alternative data preprocessing strategies to maintain a sufficient quantity of training data to enable reliable policy learning.

## 5. Conclusion

The experimental results presented in this work demonstrate that diffusion policies can achieve stable convergence and high success rates in a building-scale contact-rich assembly task representative of real-world construction. In Phase 1, we established a baseline by identifying parameter settings capable of achieving 100% average success rate in a deterministic mortise and tenon joint assembly task. In Phase 2, we evaluated policy robustness under controlled fabrication uncertainties, identifying parameter configurations that improved generalization to offsets of the mortise position, quantifying the critical role of force/torque feedback, and determining the demonstration quantity threshold necessary for reliable performance.

Together, these findings address the study’s core objectives: they validate the applicability of diffusion policies to building-scale robotic assembly and systematically characterize their robustness under fabrication uncertainty. Beyond the performative metrics, the experiments also yielded actionable insights for parameter tuning, sensor fusion, and demonstration count, forming a generalizable methodology for future contact-rich construction and assembly tasks. By demonstrating that diffusion policies can be systematically adapted and tuned to handle fabrication uncertainties without manual intervention, this research establishes a scalable, feedback-driven robot learning framework that addresses not only the technical demands of precision assembly, but also broader industry challenges such

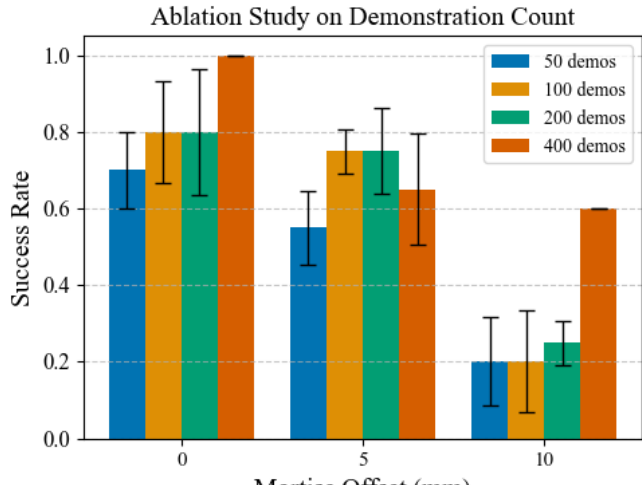


**Fig. 11.** Success rates of diffusion policies trained with different numbers of demonstrations (50, 100, 200, and 400) evaluated at three mortise offsets (0, 5, and 10 mm). Error bars indicate the standard error of the mean (SEM) computed across the 4 independently trained models for each set of parameters.

**Table 5.** Success rates for the demonstration quantity ablation study.

Policy	# Demos	$T_p$	$T_o^p$	$T_o^f$	$K_{\text{inf}}$	$\eta$	$T_a$	D (mm)	Avg. SR (%)	Avg. total SR (%)
4	400	16	1	1	32	0.5	8	0	100	75
								5	65	
								10	60	
5	<b>200</b>	16	1	1	32	0.5	8	0	80	60
								5	75	
								10	25	
6	<b>100</b>	16	1	1	32	0.5	8	0	80	58
								5	75	
								10	20	
7	<b>50</b>	16	1	1	32	0.5	8	0	70	48
								5	55	
								10	20	

D = randomized hole offset.

as labor shortages and the need to reduce reliance on physically taxing, repetitive, and high-skill manual work. Beyond timber joinery, the presented methodology can be generalized to a wide range of construction and manufacturing scenarios, from complex timber connections and pipe fitting to light metal framing, where expert craftsmanship has traditionally been essential. In doing so, this work advances robotic construction under uncertainty while contributing to safer and more efficient building practices, positioning robots as capable collaborators in the evolving construction workforce.

### 5.1. Limitations and future work

While this work demonstrates the feasibility and robustness of applying sensory–motor diffusion policy learning to contact-rich robotic assembly at construction scale, several limitations remain; our approach relies exclusively on robot pose and force data to train the policy and evaluate robustness, whereas diffusion policies for robot planning and control are commonly formulated as visuomotor policies using end-to-end mappings from RGB or tactile images to robot commands [30, 31]. Our simplification of the sensory input space increases training speed but may limit the model’s ability to generalize to visually complex or occlusion-prone construction scenarios, such as joint assembly in cluttered framing environments or alignment tasks in multi-material panel installations. Moreover, incorporating expressive state-of-the-art learning models, such as diffusion transformers or vision-language-action (VLA) models [76, 77], could enhance representation learning, enabling better generalization, scalability, and transfer across tasks. These capabilities are particularly relevant for building-scale construction where robots must integrate multiple sensing modalities and operate across varied materials, such as combining timber, metal fasteners, and composite claddings in a single assembly sequence.

Furthermore, a second limitation stems from our reliance on single-task behavior cloning from human demonstrations, which introduces both practical and algorithmic challenges. Collecting high-quality demonstrations and conducting real-world rollouts is time-intensive and can cause material degradation, especially in contact-sensitive scenarios or fragile materials like softwoods, architectural veneers, or insulation panels. Moreover, the learned policy is inherently bounded by the quality and diversity of human performance, raising the question of how to scale beyond demonstrator capabilities. This is especially critical for more dexterous and varied AEC tasks, such as assembling shingle patterns on curved surfaces, handling flexible ductwork, or manipulating deformable architectural fabrics [8, 78]. Future work could address these limitations by exploring hybrid learning paradigms that combine demonstration-based training with simulation pretraining, self-improvement cycles, or reinforcement learning, enabling policies to acquire physical reasoning skills and recover from unseen conditions [79]. Additionally, emerging research on general-purpose robot foundation models, such as visuomotor foundation models and Large Behavior Models (LBMs) [51, 79], presents a promising direction for learning transferable policies across a broad range of dexterous manipulation tasks.

### Acknowledgments

This research was supported by the National Science Foundation (NSF, Award No. 2122271), Princeton Catalysis Initiative, and the School of Architecture (SoA) at Princeton University. The authors would like to thank Ruxin Xie, Zhengyi Chen, and Roman Ibrahimov at the Adel Research Group (ARG) and SoA for their invaluable support in hardware development and data collection.

## Data availability statement

The data used in this study are available upon request.

## References

- [1] Delgado JMD, Oyedele L, Ajayi A, Akanbi L, Akinade O, Bilal M, Owolabi H. Robotics and automated systems in construction: Understanding industry-specific challenges for adoption. *Journal of Building Engineering*, 26, pp. 100868, 2019, <https://doi.org/10.1016/j.jobe.2019.100868>.
- [2] Wei HH, Zhang Y, Sun X, Chen J, Li S. Intelligent robots and human-robot collaboration in the construction industry: a review. *Journal of Intelligent Construction*, 1(1), pp. 1–12, 2023, <https://doi.org/10.26599/JIC.2023.9180002>.
- [3] Laukkonen T. Construction work and education: occupational health and safety reviewed. *Construction Management and Economics*, 17, pp. 53–62, 1999, <https://doi.org/10.1080/014461999371826>.
- [4] Arndt V, Rothenbacher D, Daniel U, Zschenderlein B, Schuberth S, Brenner H. Construction work and risk of occupational disability: a ten year follow up of 14 474 male workers. *Occupational and Environmental Medicine*, 62, pp. 559–566, 2005, <https://doi.org/10.1136/oem.2004.018135>.
- [5] Bock T. The future of construction automation: Technological disruption and the upcoming ubiquity of robotics. *Automation in Construction*, 59, pp. 113–121, 2015, <https://doi.org/10.1016/j.autcon.2015.07.022>.
- [6] Musarat MA, Alaloul WS, Rostam NAQA, Khan AM. Substitution of workforce with robotics in the construction industry: A wise or witless approach. *Journal of Open Innovation: Technology, Market, and Complexity*, 10(4), pp. 100420, 2024, <https://doi.org/10.1016/j.joitmc.2024.100420>.
- [7] Chen Z, Adel A. Advancing robotic assembly in construction: Innovations, challenges, and opportunities. *Automation in Construction*, 178, pp. 106370, 2025, <https://doi.org/10.1016/j.autcon.2025.106370>.
- [8] Graser K, Adel A, Baur M, Pont DS, Thoma A. Parallel paths of inquiry: Detailing for DFAB HOUSE. *Technology|Architecture + Design*, 5, pp. 38–43, 2021, <https://doi.org/10.1080/24751448.2021.186368>.
- [9] Adel A, Ruan D, McGee W, Mozaffari S. Feedback-driven adaptive multi-robot timber construction. *Automation in Construction*, 164, pp. 105444, 2024, <https://doi.org/10.1016/j.autcon.2024.105444>.
- [10] Willmann J, Gramazio F, Kohler M. New paradigms of the automatic robotic timber construction in architecture. In *Advancing Wood Architecture: a Computational Approach*, pp. 13–27. Routledge, 2017, <https://doi.org/10.4324/9781315678825-2>.
- [11] Apolinarska AA. *Complex timber structures from simple elements: computational design of novel bar structures for robotic fabrication and assembly*. PhD thesis, ETH Zurich, 2018, <https://doi.org/10.3929/ethz-b-000266723>.
- [12] Adel A, Thoma A, Helmreich M, Gramazio F, Kohler M. Design of robotically fabricated timber frame structures. In *Recalibration, On Imprecision and Infidelity, Proceedings of the 38th Annual Conference of the Association for Computer Aided Design in Architecture (ACADIA)*, pp. 394–403. CumInCAD, 2018, <https://doi.org/10.52842/conf.acadia.2018.394>.
- [13] Adel A. *Computational Design for Cooperative Robotic Assembly of Nonstandard Timber Frame Buildings*. PhD thesis, ETH Zurich, 2020, <https://doi.org/10.3929/ethz-b-000439443>.
- [14] Adel A. Co-robotic assembly of nonstandard timber structures. In *Hybrids & Haeccities, Proceedings of the 42nd Annual Conference of the Association for Computer Aided Design in Architecture (ACADIA)*, pp. 604–613. CumInCAD, 2022, <https://doi.org/10.7302/8675>.
- [15] Chai H, Wagner HJ, Guo Z, Qi Y, Menges A, Yuan PF. Computational design and on-site mobile robotic construction of an adaptive reinforcement beam network for cross-laminated timber slab panels. *Automation in Construction*, 142, pp. 104536, 2022, <https://doi.org/10.1016/j.autcon.2022.104536>.
- [16] Lauer APR, Benner E, Stark T, Klassen S, Abolhasani S, Schroth L, Gieniger A, Wagner HJ, Schwieger V, Menges A et al. Automated on-site assembly of timber buildings on the example of a biomimetic shell. *Automation in Construction*, 156, pp. 105118, 2023, <https://doi.org/10.1016/j.autcon.2023.105118>.
- [17] Leung PY, Apolinarska AA, Tanadini D, Gramazio F, Kohler M. Automatic assembly of jointed timber structure using distributed robotic clamps. In *PROJECTIONS, Proceedings of the 26th International Conference of the Association for Computer-Aided Architectural Design (CAADRIA)*, volume 1, pp. 583–592. CumInCAD, 2021, <https://doi.org/10.52842/conf.caadria.2021.1.583>.
- [18] Suomalainen M, Karayannidis Y, Kyrki V. A survey of robot manipulation in contact. *Robotics and Autonomous Systems*, 156, pp. 104224, 2022, <https://doi.org/10.1016/j.robot.2022.104224>.
- [19] Apolinarska AA, Pacher M, Li H, Cote N, Pastrana R, Gramazio F, Kohler M. Robotic assembly of timber joints using reinforcement learning. *Automation in Construction*, 125, pp. 103569, 2021, <https://doi.org/10.1016/j.autcon.2021.103569>.
- [20] Kramberger A, Kunic A, Iturrate I, Sloth C, Naboni R, Schlette C. Robotic assembly of timber structures in a human-robot collaboration setup. *Frontiers in Robotics and AI*, 8, pp. 768038, 2022, <https://doi.org/10.3389/frobt.2021.768038>.
- [21] Yang X, Amtsberg F, Sedlmair M, Menges A. Challenges and potential for human–robot collaboration in timber prefabrication. *Automation in Construction*, 160, pp. 105333, 2024, <https://doi.org/10.1016/j.autcon.2024.105333>.
- [22] Benson T. *Building the timber frame house: The revival of a forgotten craft*. Simon and Schuster, 1981.
- [23] Fang D, Mueller C. Mortise-and-tenon joinery for modern timber construction: Quantifying the embodied carbon of an alternative structural connection. *Architecture, Structures and Construction*, 3(1), pp. 11–24, 2023, <https://doi.org/10.1007/s44150-021-00018-5>.
- [24] Fang D. Mortise-and-tenon joinery for modern timber construction: Quantifying the embodied carbon of an alternative structural connection. Master's thesis, Massachusetts Institute of Technology, 2021, <https://hdl.handle.net/1721.1/145614>.
- [25] Levine S, Finn C, Darrell T, Abbeel P. End-to-end training of deep visuomotor policies. *Journal of Machine Learning Research*, 17(39), pp. 1–40, 2016, <http://jmlr.org/papers/v17/15-522.html>.
- [26] Finn C, Yu T, Zhang T, Abbeel P, Levine S. One-shot visual imitation learning via meta-learning. In *Proceedings of the Conference on Robot Learning CoRL*, pp. 357–368. PMLR, 2017, <https://proceedings.mlr.press/v78/finn17a.html>.
- [27] Levine S, Pastor P, Krizhevsky A, Ibarz J, Quillen D. Learning hand-eye coordination for robotic grasping with deep learning and large-scale data collection. *The International journal of robotics research*, 37(4-5), pp. 421–436, 2018, <https://doi.org/10.1177/0278364917710318>.
- [28] Kalashnikov D, Irpan A, Pastor P, Ibarz J, Herzog A, Jang E, Quillen D, Holly E, Kalakrishnan M, Vanhoucke V et al. Scalable deep reinforcement learning for vision-based robotic manipulation. In *Proceedings of Conference on robot learning (CoRL)*, volume 87, pp. 651–673. PMLR, 2018, <https://proceedings.mlr.press/v87/kalashnikov18a.html>.
- [29] Brohan A, Brown N, Carbajal J, Chebotar Y, Dabis J, Finn C, Gopalakrishnan K, Hausman K, Herzog A, Hsu J, Ibarz J, Ichter B, Irpan A, Jackson T, Jesmonth S, Joshi NJ, Julian R, Kalashnikov D, Kuang Y, Leal I, Lee KH, Levine S, Lu Y, Malla U, Manjunath D, Mordatch I, Nachum O, Parada C, Peralta J, Perez E, Pertsch K, Quiambao J, Rao K, Ryoo M, Salazar G, Sanketi P, Sayed K, Singh J, Sontakke S, Stone A, Tan C, Tran H, Vanhoucke V, Vega S, Vuong Q, Xia F, Xiao T, Xu P, Xu S, Yu T,

Zitkovich B. RT-1: Robotics transformer for real-world control at scale, 2023, <https://arxiv.org/abs/2212.06817>.

[30] Chi C, Xu Z, Feng S, Cousineau E, Du Y, Burchfiel B, Tedrake R, Song S. Diffusion policy: Visuomotor policy learning via action diffusion. *The International Journal of Robotics Research*, pp. 02783649241273668, 2024, <https://doi.org/10.1177/02783649241273668>.

[31] Chi C, Xu Z, Pan C, Cousineau E, Burchfiel B, Feng S, Tedrake R, Song S. Universal manipulation interface: In-the-wild robot teaching without in-the-wild robots, 2024, <https://arxiv.org/abs/2402.10329>.

[32] Hou Y, Liu Z, Chi C, Cousineau E, Kuppuswamy N, Feng S, Burchfiel B, Song S. Adaptive compliance policy: Learning approximate compliance for diffusion guided control, 2025, <https://arxiv.org/abs/2410.09309>.

[33] Yang L, Suh HJT, Zhao T, Graesdal BP, Kelestemur T, Wang J, Pang T, Tedrake R. Physics-driven data generation for contact-rich manipulation via trajectory optimization, 2025, <https://arxiv.org/abs/2502.00382>.

[34] Zhu H, Zhao T, Ni X, Wang J, Fang K, Righetti L, Pang T. Should we learn contact-rich manipulation policies from sampling-based planners? *IEEE Robotics and Automation Letters*, 10(6), pp. 6248–6255, 2025, <https://doi.org/10.1109/LRA.2025.3564701>.

[35] Stadelmann L, Sandy T, Thoma A, Buchli J. End-effector pose correction for versatile large-scale multi-robotic systems. *IEEE Robotics and Automation Letters*, 4, pp. 546–553, 2019, <https://doi.org/10.1109/LRA.2019.2891499>.

[36] Gandia A, Gramazio F, Kohler M. Tolerance-aware design of robotically assembled spatial structures. In *Hybrids & Haecceities, Proceedings of the 42nd Annual Conference of the Association for Computer Aided Design in Architecture (ACADIA)*, pp. 4–23. CumInCAD, 2022, [https://papers.cumincad.org/cgi-bin/works>Show?acadia22\\_4](https://papers.cumincad.org/cgi-bin/works>Show?acadia22_4).

[37] Helm V, Knauss M, Kohlhammer T, Gramazio F, Kohler M. Additive robotic fabrication of complex timber structures. In *Advancing Wood Architecture: A Computational Approach*, pp. 29–44. Routledge, 2016, <https://doi.org/10.4324/9781315678825-3>.

[38] Ruan D, McGee W, Adel A. Reducing uncertainty in multi-robot construction through perception modelling and adaptive fabrication. In *Proceedings of 40th International Symposium on Automation and Robotics in Construction (ISARC)*, pp. 25–31. IAARC Publications, 2023, <https://doi.org/10.22260/ISARC2023/0006>.

[39] Cote N, Tish D, Koehle M, Koga Y, Chitta S. Adaptive robotic construction of wood frames. *Construction Robotics*, 8(1), pp. 8, 2024, <https://doi.org/10.1007/s41693-024-00122-0>.

[40] Helmreich M, Mayer H, Pacher M, Nakajima T, Kuroki M, Tsubata S, Gramazio F, Kohler M. Robotic assembly of modular multi-storey timber-only frame structures using traditional wood joinery. In *Proceedings of the 27th International Conference for the Association for Computer-Aided Architectural Design Research in Asia (CAADRIA)*, pp. 111–120. CumInCAD, 2022, <https://doi.org/10.52842/conf.caadria.2022.2.111>.

[41] Albu-Schäffer A, Ott C, Hirzinger G. A unified passivity-based control framework for position, torque and impedance control of flexible joint robots. *The international journal of robotics research*, 26(1), pp. 23–39, 2007, <https://doi.org/10.1177/0278364907073776>.

[42] Suárez-Ruiz F, Zhou X, Pham QC. Can robots assemble an ikea chair? *Science Robotics*, 3(17), pp. eaat6385, 2018, <https://doi.org/10.1126/scirobotics.aat6385>.

[43] Vecerik M, Sushkov O, Barker D, Rothörl T, Hester T, Scholz J. A practical approach to insertion with variable socket position using deep reinforcement learning. In *2019 international conference on robotics and automation (ICRA)*, pp. 754–760. IEEE, 2019, <https://doi.org/10.1109/ICRA.2019.8794074>.

[44] Schoettler G, Nair A, Luo J, Bahl S, Ojea JA, Solowjow E, Levine S. Deep reinforcement learning for industrial insertion tasks with visual inputs and natural rewards. In *Proceedingd of 2020 IEEE/RSJ International Conference on Intelligent Robots and Systems (IROS)*, pp. 5548–5555. IEEE, 2020, <https://doi.org/10.1109/IROS45743.2020.9341714>.

[45] Johannsmeier L, Gerchow M, Haddadin S. A framework for robot manipulation: Skill formalism, meta learning and adaptive control. In *International Conference on Robotics and Automation (ICRA)*, pp. 5844–5850. IEEE, 2019, <https://doi.org/10.1109/ICRA.2019.8793542>.

[46] Robeller C, Weinand Y, Helm V, Thoma A, Gramazio F, Kohler M. Robotic integral attachment. In *Proceedings of Fabricate 2017: Rethinking Design and Construction*, volume 3, pp. 92–97. UCL Press, 2017, <https://doi.org/10.2307/j.ctt1n7qkg7.16>.

[47] Rogeau NHPL. *Robotic Assembly of Integrally-Attached Timber Plate Structures: From Computational Design to Automated Construction*. PhD thesis, EPFL, 2023, <https://infoscience.epfl.ch/entities/publication/6fd77403-f912-4f03-a68c-18a3bac91960>.

[48] Seo M, Han S, Sim K, Bang SH, Gonzalez C, Senthil L, Zhu Y. Deep imitation learning for humanoid loco-manipulation through human teleoperation. In *2023 IEEE-RAS 22nd International Conference on Humanoid Robots (Humanoids)*, pp. 1–8, 2023, <https://doi.org/10.1109/Humanoids57100.2023.10375203>.

[49] Wang C, Fan L, Sun J, Zhang R, Fei-Fei L, Xu D, Zhu Y, Anandkumar A. Mimicplay: Long-horizon imitation learning by watching human play. In *Proceedings of The 7th Conference on Robot Learning (CoRL)*, volume 229, pp. 201–221, 2023, <https://doi.org/10.48550/arXiv.2302.12422>.

[50] Shaw K, Bahl S, Pathak D. Videodex: Learning dexterity from internet videos. In Liu K, Kulic D, Ichnowski J, editors, *Proceedings of The 6th Conference on Robot Learning*, volume 205 of *Proceedings of Machine Learning Research*, pp. 654–665. PMLR, 14–18 Dec 2023, <https://proceedings.mlr.press/v205/shaw23a.html>.

[51] Zhao TZ, Kumar V, Levine S, Finn C. Learning fine-grained bimanual manipulation with low-cost hardware. In *Proceedings of Robotics: Science and Systems XIX*. Robotics: Science and Systems Foundation, 2023, <https://www.roboticsproceedings.org/rss19/p016.pdf>.

[52] Zhao TZ, Tompson J, Driess D, Florence P, Ghasemipour SKS, Finn C, Wahid A. ALOHA unleashed: A simple recipe for robot dexterity. In Agrawal P, Kroemer O, Burgard W, editors, *Proceedings of The 8th Conference on Robot Learning*, volume 270 of *Proceedings of Machine Learning Research*, pp. 1910–1924. PMLR, 06–09 Nov 2025, <https://proceedings.mlr.press/v270/zhao25b.html>.

[53] Ze Y, Zhang G, Zhang K, Hu C, Wang M, Xu H. 3d diffusion policy: Generalizable visuomotor policy learning via simple 3d representations. In *ICRA 2024 Workshop on 3D Visual Representations for Robot Manipulation*, 2024, <https://www.roboticsproceedings.org/rss20/p067.pdf>.

[54] Ho J, Jain A, Abbeel P. Denoising diffusion probabilistic models. In *Proceedings of the 34th International Conference on Neural Information Processing Systems (NeurIPS)*, volume 33, pp. 6840–6851, 2020, <https://doi.org/10.48550/arXiv.2006.11239>.

[55] Sohl-Dickstein J, Weiss E, Maheswaranathan N, Ganguli S. Deep unsupervised learning using nonequilibrium thermodynamics. In *Proceedings of the 32nd International Conference on Machine Learning*, volume 37 of *Proceedings of Machine Learning Research*, pp. 2256–2265. PMLR, 07–09 Jul 2015, <https://proceedings.mlr.press/v37/sohl-dickstein15.html>.

[56] Song J, Meng C, Ermon S. Denoising diffusion implicit models, 2022, <https://doi.org/10.48550/arXiv.2010.02502>.

[57] Florence P, Manuelli L, Tedrake R. Self-supervised correspondence in visuomotor policy learning. *IEEE Robotics and Automation Letters*, 5 (2), pp. 492–499, 2020, <https://doi.org/10.1109/LRA.2019.2956365>.

[58] Shafiuallah NM, Cui Z, Altanzaya AA, Pinto L. Behavior transformers: Cloning k modes with one stone. In Koyejo S, Mohamed S, Agarwal A, Belgrave D, Cho K, Oh A, editors, *Proceedings of Advances in Neural Information Processing Systems (NeurIPS)*, volume 35, pp. 22955–22968. Curran Associates, Inc., 2022, [https://proceedings.neurips.cc/paper\\_files/paper/2022/file/90d17e882adbda42349db6f5](https://proceedings.neurips.cc/paper_files/paper/2022/file/90d17e882adbda42349db6f5)

[0123817-Paper-Conference.pdf](#).

[59] Florence P, Lynch C, Zeng A, Ramirez OA, Wahid A, Downs L, Wong A, Lee J, Mordatch I, Tompson J. Implicit behavioral cloning. In *Proceedings of the Conference on Robot Learning (CoRL)*, pp. 158–168. PMLR, 2022, <https://proceedings.mlr.press/v164/florence22a.html>.

[60] Jarrett D, Bica I, van der Schaar M. Strictly batch imitation learning by energy-based distribution matching. In *Proceedings of Advances in Neural Information Processing Systems (NeurIPS)*, volume 33, pp. 7354–7365, 2020, [https://proceedings.neurips.cc/paper\\_files/paper/2020/hash/524f141e189d2a00968c3d48cadd4159-Abstract.html](https://proceedings.neurips.cc/paper_files/paper/2020/hash/524f141e189d2a00968c3d48cadd4159-Abstract.html).

[61] Kang JH, Joshi S, Huang R, Gupta SK. Robotic compliant object prying using diffusion policy guided by vision and force observations. *IEEE Robotics and Automation Letters*, 10(6), pp. 5505–5512, 2025, <https://doi.org/10.1109/LRA.2025.3553689>.

[62] Wu Y, Chen Z, Wu F, Chen L, Zhang L, Bing Z, Swikir A, Haddadin S, Knoll A. Tacdiffusion: Force-domain diffusion policy for precise tactile manipulation, 2025, <https://arxiv.org/abs/2409.11047>.

[63] ABB Group. IRB 4600 40kg/2,55m, <https://new.abb.com/products/robotics/robots/articulated-robots/irb-4600>. Accessed October 21, 2024.

[64] ATI Industrial Automation. F/T Sensor: Delta IP60, [https://www.ati-ia.com/products/ft/ft\\_models.aspx?id=delta+ip60](https://www.ati-ia.com/products/ft/ft_models.aspx?id=delta+ip60). Accessed October 21, 2024.

[65] Schunk. OPR 081-P00 Anti-collision and overload protection sensor, [https://schunk.com/us/en/automation-technology/anti-collision-unit/opr/c/PGR\\_1105](https://schunk.com/us/en/automation-technology/anti-collision-unit/opr/c/PGR_1105). Accessed October 21, 2024.

[66] ABB Robotics. *Technical Reference Manual - RAPID Instructions, Functions and Data Types*. ABB AB, Robotics and Motion, Västerås, Sweden, 2017. RobotWare 6.05.

[67] Beckhoff. CX2062 | Embedded PC with Intel® Xeon® D-1548. <https://www.beckhoff.com/en-us/products/ipc/embedded-pcs/cx20x2-intel-r-xeon-r-d/cx2062.html>. Accessed: 2025-05-08.

[68] Open Robotics. ROS 2 Jazzy Jalisco, 2023, <https://docs.ros.org/en/jazzy/>. Accessed: 2025-05-08.

[69] HTC Corporation. HTC VIVE Pro 2, <https://www.vive.com/us/product/vive-pro2/overview/>. Accessed October 21, 2024.

[70] Valve Corporation. OpenVR SDK, 2024, <https://github.com/ValveSoftware/openvr>. Accessed: 2025-05-12.

[71] Butterworth S. On the theory of filter amplifiers. *Wireless Engineer*, 7 (6), pp. 536–541, 1930.

[72] van den Bogert W, Iyengar M, Fazeli N. Built different: Tactile perception to overcome cross-embodiment capability differences in collaborative manipulation, 2024, <https://arxiv.org/abs/2409.14896>.

[73] Zhou Y, Barnes C, Lu J, Yang J, Li H. On the continuity of rotation representations in neural networks. In *Proceedings of the IEEE/CVF conference on computer vision and pattern recognition*, pp. 5745–5753, 2019, [https://openaccess.thecvf.com/content\\_CVPR\\_2019/papers/Zhou\\_On\\_the\\_Continuity\\_of\\_Rotation\\_Representations\\_in\\_Neural\\_Networks\\_CVPR\\_2019\\_paper.pdf](https://openaccess.thecvf.com/content_CVPR_2019/papers/Zhou_On_the_Continuity_of_Rotation_Representations_in_Neural_Networks_CVPR_2019_paper.pdf).

[74] Nichol AQ, Dhariwal P. Improved denoising diffusion probabilistic models. In *Proceedings of the 38th International Conference on Machine Learning*, volume 139 of *Proceedings of Machine Learning Research*, pp. 8162–8171. PMLR, 18–24 Jul 2021, <https://proceedings.mlr.press/v139/nichol21a.html>.

[75] Lee MA, Zhu Y, Zachares P, Tan M, Srinivasan K, Savarese S, Fei-Fei L, Garg A, Bohg J. Making sense of vision and touch: Learning multimodal representations for contact-rich tasks. *IEEE Transactions on Robotics*, 36 (3), pp. 582–596, 2020, <https://doi.org/10.1109/TRO.2019.2959445>.

[76] Octo Model Team, Ghosh D, Walke H, Pertsch K, Black K, Mees O, Dasari S, Hejna J, Kreiman T, Xu C, Luo J, Tan YL, Chen LY, Sanketi P, Vuong Q, Xiao T, Sadigh D, Finn C, Levine S. Octo: An open-source generalist robot policy, 2024, <https://arxiv.org/abs/2405.12213>.

[77] Kim MJ, Pertsch K, Karamcheti S, Xiao T, Balakrishna A, Nair S, Rafailov R, Foster E, Lam G, Sanketi P, Vuong Q, Kollar T, Burchfiel B, Tedrake R, Sadigh D, Levine S, Liang P, Finn C. OpenVLA: An open-source vision-language-action model, 2024, <https://arxiv.org/abs/2406.09246>.

[78] Craney R, Adel A. Engrained performance: Performance-driven computational design of a robotically assembled shingle facade system. In *Distributed Proximities, Proceedings of the 40th Annual Conference of the Association of Computer Aided Design in Architecture (ACADIA)*, pp. 604–613. CumInCAD, 2020, <https://doi.org/10.52842/conf.acadia.2020.1.604>.

[79] TRI LBM Team, Barreiros J, Beaulieu A, Bhat A, Cory R, Cousineau E, Dai H, Fang CH, Hashimoto K, Irshad MZ, Itkina M, Kuppuswamy N, Lee KH, Liu K, McConachie D, McMahon I, Nishimura H, Phillips-Grafflin C, Richter C, Shah P, Srinivasan K, Wulfe B, Xu C, Zhang M, Alspach A, Angeles M, Arora K, Guizilini VC, Castro A, Chen D, Chu TS, Creasey S, Curtis S, Denitto R, Dixon E, Dusel E, Ferreira M, Goncalves A, Gould G, Guoy D, Gupta S, Han X, Hatch K, Hathaway B, Henry A, Hochsztien H, Horgan P, Iwase S, Jackson D, Karamcheti S, Keh S, Masterjohn J, Mercat J, Miller P, Mitiguy P, Nguyen T, Nimmer J, Noguchi Y, Ong R, Onol A, Pfannenstiel O, Poyner R, Rocha LPM, Richardson G, Rodriguez C, Seale D, Sherman M, Smith-Jones M, Tago D, Tokmakov P, Tran M, Hoorick BV, Vasiljevic I, Zakharov S, Zolotas M, Ambrus R, Fetzer-Borelli K, Burchfiel B, Kress-Gazit H, Feng S, Ford S, Tedrake R. A careful examination of large behavior models for multitask dexterous manipulation, 2025, <https://arxiv.org/abs/2507.05331>.